scientific reports

Check for updates

OPEN

Natural history of nonhuman primates after conjunctival exposure to Ebola virus

Robert W. Cross[1,2], Abhishek N. Prasad[1,2], Courtney B. Woolsey[1,2], Krystle N. Agans[1,2], Viktoriya Borisevich[1,2], Natalie S. Dobias[1,2], Jason E. Comer[1,2], Daniel J. Deer[1,2], Joan B. Geisbert[1,2], Angela L. Rasmussen[3,4], Walter Ian Lipkin[3], Karla A. Fenton[1,2] & Thomas W. Geisbert[1,2]✉

Transmission of Ebola virus (EBOV) primarily occurs via contact exposure of mucosal surfaces with infected body fluids. Historically, nonhuman primate (NHP) challenge studies have employed intramuscular (i.m.) or small particle aerosol exposure, which are largely lethal routes of infection, but mimic worst-case scenarios such as a needlestick or intentional release, respectively. When exposed by more likely routes of natural infection, limited NHP studies have shown delayed onset of disease and reduced mortality. Here, we performed a series of systematic natural history studies in cynomolgus macaques with a range of conjunctival exposure doses. Challenge with 10,000 plaque forming units (PFU) of EBOV was uniformly lethal, whereas 5/6 subjects survived lower dose challenges (100 or 500 PFU). Conjunctival challenge resulted in a protracted time-to death compared to i.m. Asymptomatic infection was observed in survivors with limited detection of EBOV replication. Inconsistent seropositivity in survivors may suggest physical or natural immunological barriers are sufficient to prevent widespread viral dissemination.

Filoviruses, including Ebola virus (EBOV) and Marburg virus (MARV), are responsible for periodic outbreaks of viral hemorrhagic fever with case fatality rates of up to 90%[1]. Historically, filoviruses have caused relatively small outbreaks ranging from one case to a few hundred cases with limited geographic spread[1]. The 2013–2016 West African epidemic of EBOV (variant Makona) represented a departure from this pattern, with over 28,000 cases and 11,000 deaths[2]. More recently, the resolved 2018–2020 outbreak of EBOV (variant Ituri)[3] in the Democratic Republic of the Congo (DRC) resulted in at least 3481 cases and 2299 deaths[4]. The increased scale, duration, and geographic footprint of these outbreaks emphasize the gaps in understanding the variety of modes of human-to-human transmission of filoviruses. While fractured healthcare systems, socio-political unrest, and security issues are known to contribute to spread of the virus, clarification is needed in the specific role different routes of infection play in the kinetics of virus transmission and disease progression, particularly in mild, asymptomatic, or recrudescent cases.

Irrespective of scale, filovirus outbreaks in humans are frequently traced back to a single episode of zoonotic transmission, after which human-to-human transmission drives the remainder of the outbreak[5]. Instances of multiple zoonotic introductions within a single MARV outbreak have also been reported[6,7]. Egyptian rousette bats (*Rousettus aegyptiacus*) play a role in the natural maintenance of MARV[8], and several species of frugivorous and insectivorous bats have been implicated, but not confirmed, as potential reservoir species for EBOV[9]. In addition, secondary species, such as nonhuman primates (NHP) and duikers have been speculated to facilitate spillover of EBOV into humans[10]. Recently, a case study from the 2018–2020 outbreak in North Kivu, DRC demonstrated that humans themselves may act as reservoirs post-convalescence, and can ignite further outbreaks following recrudescence of symptomatic disease at least 6 months following the initial recovery[11] and may even take years to manifest, as observed in a recent resurgence in Guinea[12]. Intramuscular (i.m.) inoculation through the re-use of needles in a clinical setting fueled the spread of EBOV during the initial outbreak in Yambuku, DRC in 1976[13], but has not played a major role in subsequent outbreaks. Still, percutaneous/parenteral exposure via

[1]Department of Microbiology and Immunology, University of Texas Medical Branch, Galveston, TX 77550, USA. [2]Galveston National Laboratory, University of Texas Medical Branch, Galveston, TX 77550, USA. [3]Center for Infection and Immunity, Columbia Mailman School of Public Health, New York, NY 10032, USA. [4]Vaccine and Infectious Disease Organization, University of Saskatchewan, Saskatoon, SK, Canada. ✉email: twgeisbe@utmb.edu

needlestick injury is an ever-present hazard to personnel in both research and clinical environments[14–17]. Routes of infection in cases with no documented needle use are less clear, but presumed to involve mucosal surfaces (e.g., conjunctival, oral, nasal, or sexual exposure)[18]. EBOV is found in a variety of bodily fluids including saliva, blood, stool, breast milk, and semen. This suggests the primary risk factor for human-to-human transmission is mucosal contact with body fluids from infected persons[19].

A clear understanding of the natural history of different routes of infection is critical for understanding the epidemiology of pathogenic agents and for the development of medical countermeasures. This is particularly important in the case of filovirus disease, as most preclinical development and validation efforts of vaccines and therapeutics in animal models, such as NHPs, have demonstrated protection against i.m. injection or small particle aerosol rather than mucosal exposures that mimic natural infections (e.g. conjunctival, oral, nasal, sexual). Thus, it is largely unknown how the protective efficacy of these countermeasures may be impacted by different routes of filovirus infection. While implementation of the US Food and Drug Administration-approved EBOV vaccine ERVEBO has had clear benefit in the management of EBOV outbreaks[20], there is still much to be learned regarding what impacts mucosal exposure have on medical countermeasure efficacy.

NHPs have historically been used as the animal model of choice against filoviruses as they recapitulate the most salient features of fatal human EBOV disease (EVD)[21]. Previous work has demonstrated that low doses (0.01–50 PFU) of EBOV or MARV delivered by i.m. injection cause lethal disease in NHPs[22–25]. However, in rare instances, rhesus macaques have survived i.m. challenge with doses that typically produce lethality in NHPs (e.g. 1000 PFU); it should be noted that this appears to be associated with virus seed stocks exhibiting the 8U editing site genotype[21]. Limited data exist characterizing the required doses needed to cause an infection. Moreover, the natural history of mucosal infection by filoviruses in NHPs is less understood than for more conventional challenge models (*e.g.* i.m..). A recent study reported a protracted disease course in cynomolgus macaques following intranasal (i.n.) challenge with low doses (10 and 100 PFU) of the Kikwit isolate of EBOV[26]. Conversely, conjunctival challenge of ferrets with low doses (1, 10, or 100 PFU) of EBOV-Kikwit failed to produce evidence of productive infection, in contrast to the uniform lethality observed via oronasal and oral challenge routes in this same model[27]. Several studies have examined small particle aerosol challenge to understand disease processes and to evaluate medical countermeasures in the context of an intentional filovirus release[28–31]. Alfson et al. characterized an EBOV i.n. challenge model using a large particle generating atomizer, a model more reflective of person-to-person airborne droplet transmission[32]. In this study, disease progression was delayed compared to i.m. challenge with the large particle but not small particle aerosol challenge. These results suggest the virus faces additional physical and/or immunological barriers to infection via inhalational or mucosal routes associated with droplet size. Two studies have examined a range of infectious doses in both rhesus and cynomolgus macaques by the oral and conjunctival routes[33,34]; however, the outcomes were limited by the narrow scope and small group sizes in both studies. The work here represents a systematic extension of previous work in cynomolgus monkeys. Here, we add to the body of knowledge concerning the natural history of lethal disease and survival to three different doses of conjunctival exposure to EBOV using the 2013–2016 epidemic Makona variant.

Results

Experimental infection of cynomolgus macaques with EBOV via the conjunctival route.
We exposed three groups (n = 6 animals/group) of healthy, adult cynomolgus macaques with a target dose of 100 (actual dose 115), 500 (actual dose 475), or 10,000 (actual dose 9625) PFU of EBOV via the conjunctiva. Across all dosage cohorts, only animals that progressed to fatal disease exhibited sustained fever followed by progressive hypothermia (Fig. S1). In both lower dose cohorts, surviving animals (5/6 per group) showed minimal clinical signs of disease, with decreased food intake or brief anorexia being the only outward sign (Table S1). Conversely, each of the animals that developed fatal disease in these two cohorts developed classical clinical signs of EVD, including anorexia, recumbency, and petechial rash. Both animals met euthanasia criteria 11 days post-infection (dpi) (Fig. 1A). In contrast to the two lower dose groups, all the animals in the high challenge dose group developed fatal EVD, with a mean time to death (MTD) of 12.33 ± 3.25 dpi. The disease course in 3/6 animals was extended to 13–17 days, with the first signs of illness appearing 6–11 dpi, while the remaining three animals met euthanasia criteria on days 9 or 10. There was a significant difference in survival curves between the 100 and 10,000 PFU challenge cohorts (p = 0.0049, Mantel-Cox log rank test) and 500 and 10,000 PFU cohorts (p = 0.0049, Mantel-Cox log rank test), but not between the 100 and 500 PFU cohorts (p > 0.99, Mantel-Cox log rank test) (Fig. 1A). To determine whether challenge via conjunctival exposure resulted in a protracted disease course versus the i.m. route, we compared the MTD of animals that succumbed to disease across the three cohorts (MTD = 12.0 ± 3.1 dpi, n = 8) to that of unprotected positive control cynomolgus macaques challenged i.m. with typical (~ 1000 PFU) doses of the C07 isolate of EBOV Makona from several published studies (MTD = 7.1 ± 1.0 dpi, n = 18)[35–39], and found a statistically significant difference in survival time (p = 0.003, Welch's t-test) (Fig. S2).

Marked changes were observed in blood coagulation parameters (e.g., increased prothrombin time (PT) and activated partial thromboplastin time (aPTT), decreased circulating fibrinogen). These findings are indicative of severe disruption to extrinsic and intrinsic coagulation pathways (i.e., acute disseminated intravascular coagulation and liver damage/failure was observed in all fatal cases regardless of challenge dose) (Fig. S3A–C). A single surviving animal from the 500 PFU challenge cohort (subject 500-4) displayed similar deviation from baseline coagulation indices which resolved completely by 14 dpi (Fig. S3B). Predictably, all fatal cases exhibited hallmark features documented in other reports of NHP infection with EBOV regardless of dose. Dramatic changes in leukocyte populations were observed in these subjects, as well as serum markers of hepatic and renal function and inflammation, compared to those that survived (Table S1). Notably, in fatal cases, there was a lack of association between the challenge dose and the severity of disruption from baseline hematological and metabolic parameters.
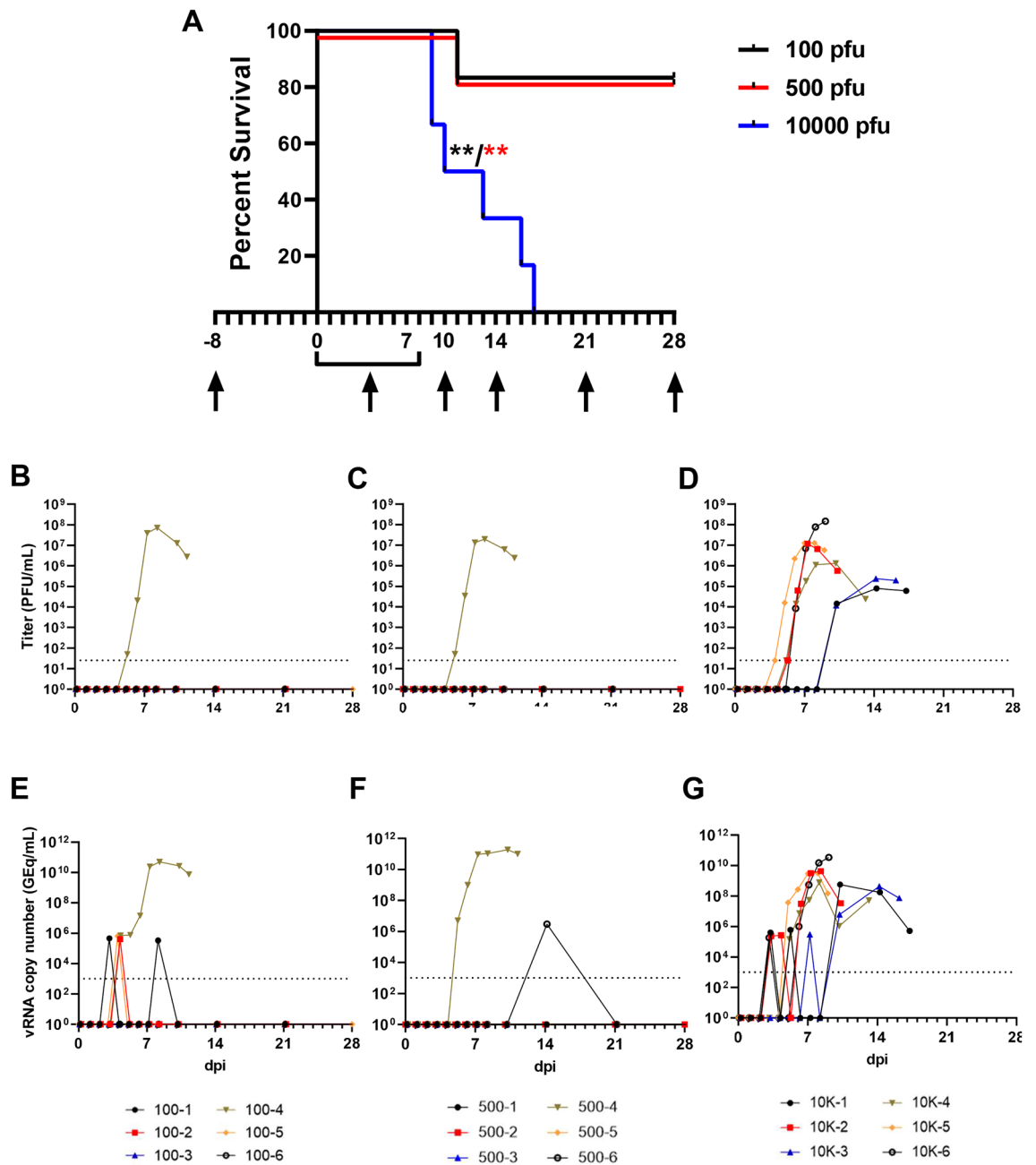
Figure 1. Survival analysis and determination of viral load in EBOV-challenged macaques. (**A**) Kaplan–Meier survival curves of cynomolgus macaques challenged with low (100–500 PFU) and high (10,000 PFU) doses of EBOV variant Makona. Arrows below x-axis denote scheduled sampling days. Colored asterisks denote statistical significance to the same colored group. **p ≤ 0.01. Viral load was determined by plaque titration of plasma (**B**–**D**) and RT-qPCR detection of EBOV vRNA (**E**–**G**) from whole blood.

Quantitation of EBOV vRNA and infectious virus load. We assessed levels of circulating infectious EBOV in plasma and EBOV RNA (vRNA) in whole blood by plaque assay and RT-qPCR, respectively. In both lower dose groups, infectious EBOV was only recovered in animals that developed fatal disease (Fig. 1B,C) while all animals developed levels of circulating infectious virus in the high dose group (Fig. 1D). In the two animals from the high dose cohort exhibiting the most protracted time-to-death (TTD) (euthanized at 16 and 17 dpi), detectable levels of circulating infectious EBOV and vRNA developed later and at lower titers than in the animals with a shorter disease course (Fig. 1D,G). Circulating vRNA was detected transiently in 3/6 and 1/6 survivors from the 100 and 500 PFU challenge cohorts, respectively (Fig. 1E,F). Tissues were collected at necropsy and assayed for the presence of vRNA and infectious EBOV. vRNA was primarily restricted to lymphoid tissue, liver, spleen, and lungs in surviving animals from the 100 PFU cohort (Fig. S4A) but was also found in low abundance (~ 10^4 Genomic Equivalents/gram (GEq/g) tissue) in the eye and transverse colon of one survivor (100-5). Similarly, vRNA was absent in most tissues from surviving animals in the 500 PFU challenge cohort; however,

two animals (500-1 and 500-6) had detectable vRNA in the gonads, and vRNA was found in the eyes from three survivors (500–1, 500-3, 500-6) (Fig. S4C). vRNA was present in similar quantities (~10^8–10^{10} GEq/g tissue) in most or all tissues from all animals which succumbed, regardless of challenge dose (Fig. S4A,C,E). Likewise, titers of infectious EBOV recovered from the tissues of animals which succumbed also did not appear to be dependent on the challenge dose (Fig. S4B,D,F). Infectious EBOV was absent, or below the limit of detection, in the pancreas of 3/6 animals (10K-4, 10K-5, 10K-6) in the 10,000 PFU challenge cohort but was recovered from all other animals that succumbed. Infectious EBOV was not recovered from any tissues assayed from surviving animals. There was no significant difference in the mean peak viral load, day of peak viremia, or day of earliest detection, whether measured by plaque assay (for fatal cases only) or RT-qPCR (for all animals with detectable vRNA), between the two lower dose groups and the high dose group (Fig. S5A,B), although fatal cases had markedly higher levels of vRNA in both blood and tissues (Fig. S5B).

Pathology.   Regardless of EBOV challenge dose, postmortem gross examination of animals which succumbed to lethal disease revealed lesions consistent with those observed in i.m. challenge models, including necrotizing hepatitis (Fig. 2B,C) characterized as hepatic pallor with reticulation [absent in surviving animals (Fig. 2A)]; splenomegaly; petechial rash on the limbs, face, and/or trunk (Fig. 2D); and hemorrhagic interstitial pneumonia characterized as failure to completely collapse and multifocal reddening of the lungs (Fig. 2E).

Macaques that succumbed to EVD displayed the expected terminal stage histologic lesions observed in i.m. and small particle aerosol-challenged animals despite different challenge doses of 100 PFU (100-4), 500 PFU (500-4), or 10,000 PFU (all animals) of EBOV. Histologic lesions occurring in all macaques that succumbed to EVD included lymphadenitis (axillary, inguinal, and mandibular lymph nodes); tonsillitis; splenitis with lymphoid depletion and fibrin deposition (Fig. 3G,M,S); multifocal necrotizing hepatitis (Fig. 3K,Q,W); and interstitial pneumonia (Fig. 3I,O,U). Other histologic lesions present in at least one macaque that succumbed to EVD included hemorrhagic interstitial pneumonia (Fig. 3U), uveitis (100-4), adrenalitis (10K-3), tracheitis and esophagitis (10K-2, 10K-3, 10K-4), myocarditis (10K-2, 10K-3), and gastritis (10K-2). Immunolabeling for anti-EBOV antigen was present in macaques that succumbed to disease in the expected cell types, which included individual to small clusters of mononuclear cells within the subcapsular and medullary spaces of the lymph nodes; medullary spaces of the tonsil; red and white pulp of the spleen (Fig. 3H,N,T); alveolar septate and frequently alveolar macrophages of all lung lobes (Fig. 3J,P,V and insets) and hepatic sinusoidal lining cells; Kupffer cells; and rarely individual hepatocytes (Fig. 3L,R,X). Immunohistochemistry (IHC)-positive mononuclear cells were often noted in lesser numbers in the interstitial tissues of the renal cortex, adrenal gland, salivary gland, pancreas, heart, testis, uterus, and prostate. Additionally, mononuclear cells were IHC positive within the dermis or submucosa of the haired skin, nasal mucosa, conjunctiva, urinary bladder, trachea, esophagus, and gastrointestinal tract. IHC-positive mononuclear cells were found within the ciliary body and the draining angle of the eye, adrenal cortical cells, theca cells of the ovary, and the endothelium of small caliber vessels within the meninges and brain parenchyma (Fig. 4E,H,K). Punctate, cytoplasmic in situ hybridization (ISH) signal for viral RNA was abundantly present in the endothelium of small caliber vessels within the brain (Fig. 4F,I,L). Mild gliosis was observed in animals that succumbed to infection from all three dosage cohorts (Fig. 4A,D,G,J), as well as in one survivor from the 100 PFU group (100-6), which was associated with a focal cluster of IHC-positive neuronal cells within the brainstem (Fig. 4A,B). Punctate, cytoplasmic ISH was scarcely present in a neuronal cell in the brainstem (Fig. 4C). No appreciable lesions or IHC labeling for anti-EBOV antigen was present in
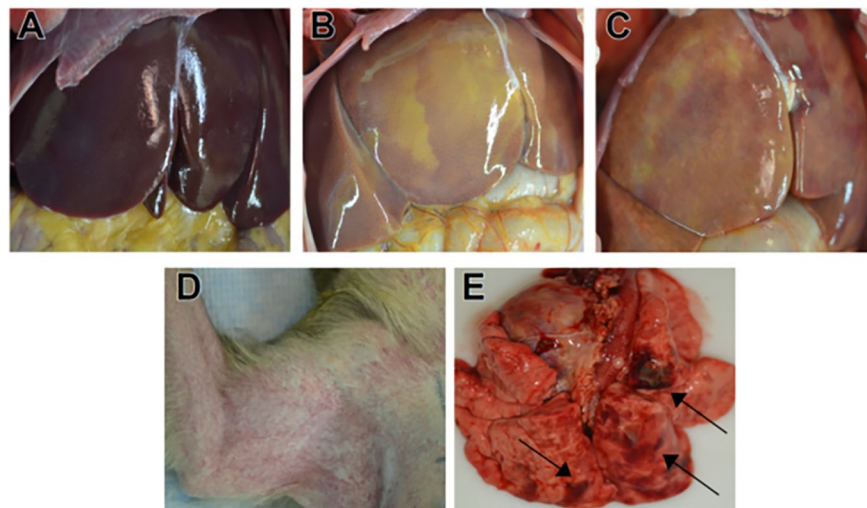

Figure 2.   Representative gross pathology in cynomolgus macaques infected with EBOV Makona variant via conjunctival route. (**A**) Lack of significant hepatic lesions in a 100PFU survivor (100-5), (**B**) marked necrotizing hepatitis (500-4), (**C**) marked diffuse necrotizing hepatitis (100-4), (**D**) marked axillary petechial rash (10K-6), (**E**) multifocal hemorrhagic interstitial pneumonia (black arrows) (10K-6).
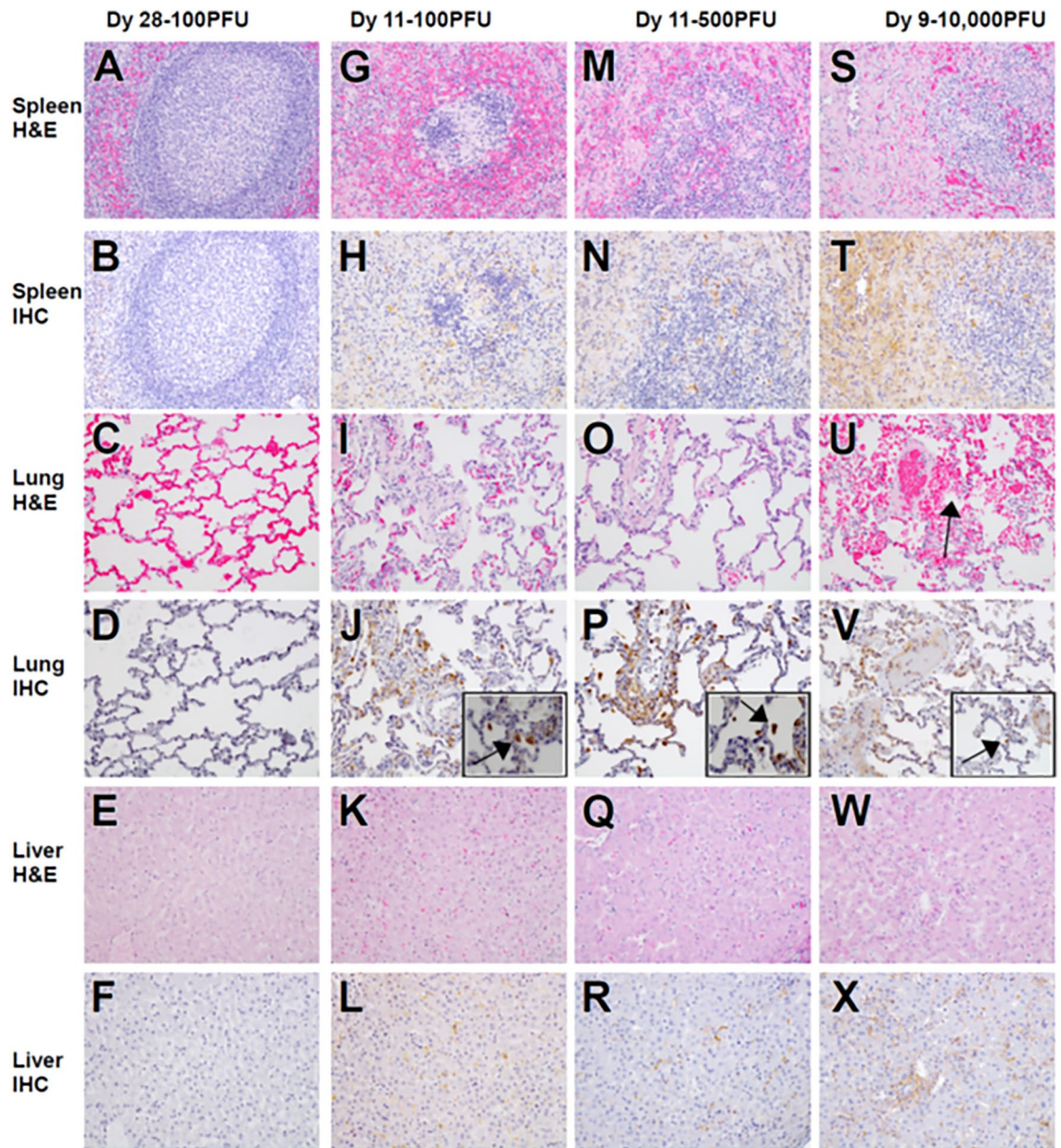
Figure 3. Representative histologic lesions in cynomolgus macaques infected with EBOV Makona variant via conjunctival route. Representative tissues of cynomolgus macaques from 100 PFU, survivor (100-6) (**A–F**) and succumbed 11 dpi (100-4) (**G–L**), 500 PFU, succumbed 11 dpi (500-4) (**M-R**) and 10,000 PFU, succumbed 9 dpi (10K-6) (**S–X**). All images captured at 20x, insets captured at 40x. Hematoxylin and eosin (H&E) staining (**A,G,M,S,C,I,O,U,E,K,Q,W**) and immunohistochemistry (IHC) for anti-EBOV antigen (**B,H,N,T,D,J,J,Inset,P,P inset,V,V inset, F,L,R,X**). No significant lesions (NSL) and no significant immunolabeling (NSI) for spleen (**A,B**), lung (**C,D**) and liver (**E,F**) of 100 PFU survivor. Splenitis with lymphoid depletion and fibrin deposition in NHPs that succumb at 100 PFU (**G**), 500 PFU (**M**) and 10,000 PFU (**S**). Diffuse cytoplasmic immunolabeling of mononuclear cells (brown) in red and white pulp of the spleen in those that succumb (**H,N,T**). Diffuse interstitial pneumonia (**I,O,U**) with alveolar hemorrhage (**U**, black arrow). Diffuse cytoplasmic immunolabeling (brown) of mononuclear cells within the lung (**J,P,V**) and alveolar spaces (insets **J,P,V**, black arrows). Necrotizing hepatitis (**K,Q,W**). Diffuse cytoplasmic immunolabeling (brown) of Kupffer cells, sinusoidal lining cells and rarely hepatocytes (**L,R,X**).

all other examined organs of this macaque (Fig. 3A–F). No prominent lesions or IHC labeling for anti-EBOV antigen were detected in examined tissues of 4/6 macaques from the 100 PFU cohort (100-1,100-2,100-3, 100-5) and 5/6 macaques from 500 PFU cohort (500-1, 500-2, 500-3, 100-5, 500-6) (data not shown).

Enzyme-linked immunosorbent assay (ELISA) detection of anti-EBOV antibodies. Terminal sera from all animals surviving to the study endpoint (28 dpi) was analyzed by ELISA and PRNT$_{50}$ for the
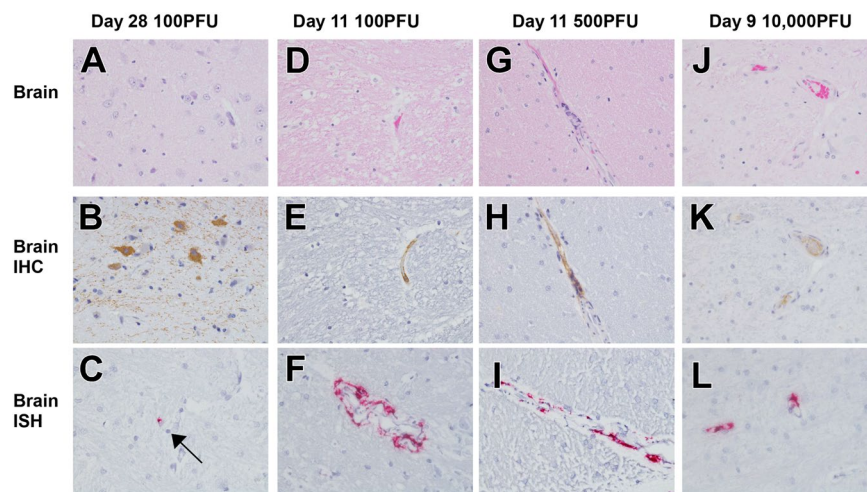
Figure 4. Representative histologic lesions in the brain of cynomolgus macaques infected with EBOV Makona variant via conjunctival route. Representative tissues of cynomolgus macaques from 100 PFU, survivor (100-6) (**A–C**) and succumbed 11 dpi (100-4) (**D–F**), 500 PFU, succumbed 11 dpi (500-4) (**G–I**) and 10,000PFU, succumbed 9 dpi (10K-6) (**J–L**). All images captured at 40×. Hematoxylin and eosin (H&E) staining (**A,D,G,J**), immunohistochemistry (IHC) for anti-EBOV antigen (**B,E,H,K**), in situ hybridization (**C,F,I,L**). Mild gliosis (**A,D,G,J**). Diffuse cytoplasmic immunolabeling for anti-EBOV antigen in neuronal cells (B, brown), endothelium of small caliber vessels (**E,H,K**). Punctate labeling (red) in a single neuronal cell of 100 PFU survivor (100-6) (c, black arrow) and endothelium of small caliber vessels (**F,I,L**).

presence of anti-EBOV antibodies and neutralizing capacity, respectively. In the 100 PFU-challenged cohort, 3/5 animals had detectable titers of anti-EBOV antibodies when assayed against either inactivated virus or GP antigen alone (Fig. S6A). Titers against inactivated virus were below the threshold for detection in all animals from the 500 PFU-challenged cohort; however, GP-specific IgG was detected in 2/6 animals from this group (Fig. S6B). Terminal sera from all surviving animals had little to no neutralizing activity against live EBOV, with none reaching the 50% plaque-reduction threshold for the assay (data not shown).

Circulating cytokine/chemokine profiling. We assessed levels of select circulating cytokines and chemokines in sera from macaques in the current study and compared them to those from a previous serial euthanasia study utilizing cynomolgus macaques inoculated i.m. with the identical isolate and seed stock of EBOV variant Makona[40]. Animals in the current study were sampled daily up to 6 dpi, providing a means of direct comparison of analyte levels during the acute phase of the disease course. For most analytes, patterns of secretion were similar between inoculation routes (Fig. 5). Notable differences in analyte levels were observed for IL-4 and IL-13, with IL-13 being elevated in macaques inoculated via the conjunctiva versus those inoculated via the i.m. route (Fig. 5I,J). Moreover, higher levels of IL-13 were observed for macaques challenged via the conjunctiva that succumbed to disease compared to those that survived (Fig. 5J).

Discussion

The development of animal models that recapitulate human diseases is critical to furthering our understanding of the underlying pathological processes and advancing medical countermeasures. NHPs have proven to be an invaluable resource in accurately modeling the clinical progression of disease, pathology, and severity of EVD in humans[21]. While sexual transmission of both EBOV and MARV has been well documented, transmission of filoviruses is largely understood to involve exposure to infected animals or via person-to-person through contact with body fluids (e.g., blood, vomitus, saliva), excreta, and possibly fomites. Incidental transmission through the facial mucosa is further facilitated through the natural inclination to habitually touch one's own face, perhaps hundreds of times per day[41–43].

Here, we designed a study with cynomolgus macaques utilizing low (100 and 500 PFU) and high (10,000 PFU) doses of EBOV variant Makona inoculated via the conjunctiva. A key observation from these studies is that challenge of macaques via the conjunctival route exhibited dose-dependent lethality with a 10,000 PFU dose resulting in uniform lethality, whereas doses of 100 and 500 PFU caused lethal disease in only 1/6 macaques in each cohort. Conversely, the duration and severity of disease in fatal cases, as well as the onset and magnitude of viremia, was not correlated with challenge dose. Surprisingly, while vRNA was detected in some or all tissues from infected subjects regardless of clinical outcome, circulating infectious EBOV was only detected in animals that succumbed to lethal disease. vRNA was found in immunologically privileged potential reservoir sites (eyes and/or gonads) from four surviving animals from the 100 and 500 PFU challenge groups; however, infectious virus was not recovered from any tissues in surviving animals. Detection of circulating vRNA in whole blood was restricted to 3/5 and 1/5 animals from the 100 and 500 PFU challenge cohorts, respectively. While some studies have demonstrated that low doses (0.01–50 PFU) of EBOV or MARV delivered i.m. are sufficient to produce
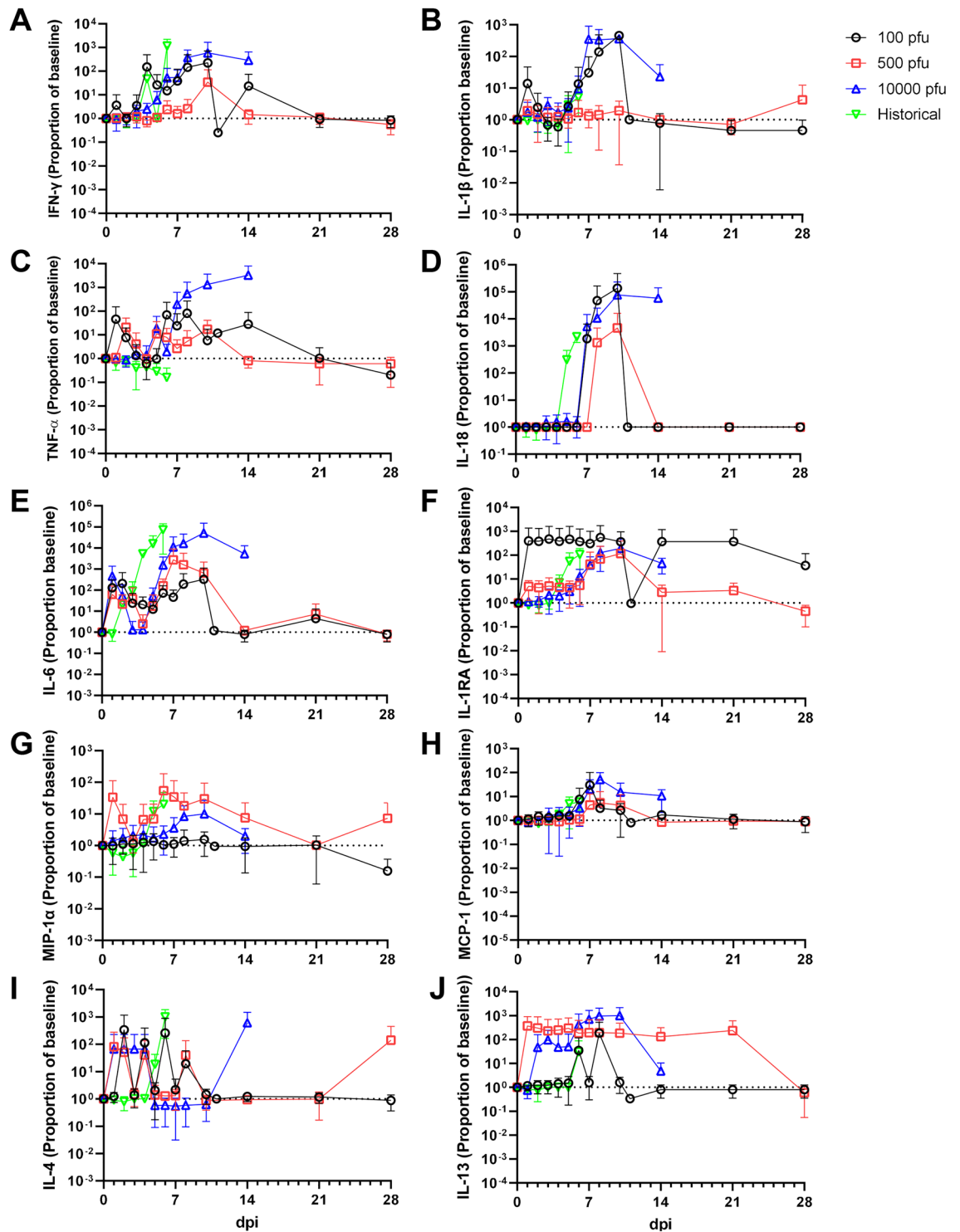
Figure 5. Circulating levels of inflammatory markers in EBOV-challenged macaques. Absolute values of each analyte measured for each subject at the indicated timepoints, and normalized to baseline (day 0/challenge) values. Shown is the average value for all animals in the indicated group. Data is shown as a proportion of baseline (set to 1, indicated by dashed horizontal line in each panel) to facilitate plotting on a log scale. Data from historical control animals inoculated i.m. with the homologous virus[40] were included for statistical purposes. (**A**) IFN-γ; (**B**) IL-1β; (**C**) TNF-α; (**D**) IL-18; (**E**) IL-6; (**F**) IL-1RA; (**G**) MIP-1α; (**H**) MCP-1; (**I**) IL-4; (**J**) IL-13. All assays were run in duplicate reactions.

lethal disease in NHPs[22–25], the work presented here suggest a higher threshold for productive infection and disease may be necessary for other mucocutaneous routes of infection with EBOV. Indeed, a comparison of the animals that succumbed to disease in our study to i.m.-challenged positive control macaques from the published literature[35–39] revealed a significant delay in time to death. In addition, Johnston et al. recently reported delayed MTD (11.1–13.0 dpi, independent of dose and method of administration) in cynomolgus macaques challenged i.n. with 10 or 100 PFU target doses of EBOV, administered either dropwise or as a large-droplet aerosol[26]. However, in contrast to the present study and a previous one utilizing 100 and 10 PFU doses[34], respectively, Johnston et al. reported near-uniform lethality across cohorts, though it should be noted a different isolate of EBOV (Kikwit) was used. Comparatively, Jaxx et. al. showed a time to death in rhesus macaques between 7–8 dpi after oral or conjunctival challenge with ~ 100,000 PFU of the Mayinga variant of EBOV[33]. This contrasts to the findings in our study where the disease onset in fatal cases was considerably delayed (9–17 dpi), although the different EBOV variant and species of macaque may influence challenge route and/or dose dependent differences. A subsequent exploratory study utilizing small cohorts of cynomolgus macaques demonstrated that low doses (10 or 100 PFU) of EBOV Makona variant delivered via the conjunctiva were non-lethal and only the 100 PFU dose demonstrated low-level viremia as well as seroconversion to the EBOV glycoprotein[34]. In our study, seroconversion in surviving animals was not uniformly observed across challenged subjects and the neutralizing activity of sera was weak to nonexistent. One possible critique of the present study and previous ones exploring conjunctival challenge in macaques and ferrets is that the low lethality, undetectable viremia, and incomplete seroconversion observed in the 100 and 500 PFU cohorts may be due to some or all of the challenge material being expelled from the conjunctiva via blinking, tear secretion, or some other means. While we cannot discount this possibility entirely, with regards to the present study, we find this unlikely given that all surviving animals had detectable EBOV vRNA in at least one tissue harvested at necropsy, indicating some degree of dissemination and replication distal to the inoculation site.

Taken together, our studies along with previous studies exploring low-dose EBOV mucosal exposure via routes likely relevant to natural transmission suggest a substantial difference in threshold for the development of lethal EVD in comparison to i.m. or small particle aerosol exposure. Different exposure routes present both advantages and challenges to productive infection, including differences in the physical and immunological interface. In addition, the matrix in which the virus is contained and its stability in the matrix may influence the likelihood of infection. For example, the most probable source of infection during natural outbreak is contact with contaminated body fluids[19], and EBOV has been experimentally estimated to be viable in liquid blood for up to 8 days, or 5 days in dried blood, in conditions modeling both clinical and tropical environments[44]. Conversely, EBOV was found to only be stable for ~ 100 min in small particle suspensions of 1–3 μm[45]. The conjunctiva is one of the most immunologically active mucosal tissues of the external eye[46,47]. While macrophages, neutrophilic granulocytes, mast cells, and lymphocytes of various lineages are known to inhabit the conjunctiva, the constitutive secretion of immunoglobulin A (IgA) provides additional barriers which may impede productive infection at lower doses. Polymeric/secretory IgA (pIgA/SIgA) can bind some viruses and bacteria leading to their recognition or neutralization by the immune system with varying specificity[48]. Additionally, tear film has anti-microbial properties due to the presence of lysozymes, lactoferrins, lipocalin, and beta-lysine, which can facilitate pathogen defenses including bacterial cell wall lysis, prevention of bacterial and viral binding, inflammation, and detoxification[47]. IgA has also been found in higher concentrations in tear film than serum[49].

We observed increased levels of circulating IL-4 and IL-13 in animals that succumbed to lethal EVD, compared to relatively low levels of IL-13 in animals that survived infection. IL-13 is a profibrotic cytokine secreted by type 2 T-helper cells (Th2), mast cells, and basophils[50], and is involved in goblet cell homeostasis in the respiratory, gastrointestinal, and conjunctival mucosa[51]. With regards to EBOV, in vitro polarization of macrophages to the M2 wound-healing subtype by combined IL-4/IL-13 administration promoted infection by a recombinant vesicular stomatitis virus (rVSV) expressing EBOV GP (rVSV/EBOV GP), but not the parental rVSV vector[52]. Similarly, in vivo treatment or ex vivo treatment and implantation of macrophages with IL-4/IL-13 increased disease severity and mortality in mice challenged with rVSV/EBOV GP[52]. While the IL-13 and IL-4 we measured was systemic, and not localized to the ocular interface, the patterns of expression we observed in this study differed from those observed during the acute phase of infection in i.m.-inoculated macaques[40], indicating the possibility of a unique role of these cytokines in EBOV pathogenesis via the conjunctival or other mucosal portals. Immunological skewing towards a Th2 phenotype has also been observed to play a role in lethality to MARV infection[53].

The recent re-emergence of EBOV in Guinea 6 years after the end of the West African epidemic underpins the importance of understanding pathogenesis and mechanisms of viral clearance as the index case was determined to most likely be recrudescence event from an otherwise recovered patient[12]. A subsequent study from the 2018–2020 North Kivu outbreak in DRC confirmed fatal recrudescence in the index case of an outbreak that resulted in an additional 91 human infections[11]. Modeling the complexities associated with survival to filovirus disease in NHPs affords unique opportunities, but is not without challenges, central of which is the enormous effort and lack of space to conduct long-term studies in high containment facilities. Nonetheless, the value of NHP survivor studies from natural infection or therapeutic studies, particularly when treatment is not initiated until advanced disease, cannot be understated. Recently, a number of studies with survivors from therapeutic EBOV studies in NHPs demonstrated evidence that replicating virus may still be present in sanctuary sites, which are largely immune privileged sites throughout the body, that may still allow for shedding of infectious virus despite potent circulating cellular and humoral immunity[54]. These sites include reproductive, ocular, and central nervous systems (CNS), all for which evidence has been observed in humans[55–58]. In this study, we provide evidence of replicating virus in the CNS tissues in the context of survival from uninterrupted natural infection.

With a few exceptions, much of the preclinical work for medical countermeasures, including ERVEBO, has utilized the i.m. challenge model[59]. While certainly important by representing the high-risk scenario of a

needle-stick in the hospital or laboratory setting, it is not truly representative of transmission during a natural outbreak, which more likely involves exposure of mucosal surfaces to infected body fluids or excreta. This becomes particularly important with respect to postexposure treatments where the therapeutic window of i.m. versus mucosal challenge with filoviruses are not equivalent.

While some descriptions of survivor models of EBOV infection in the context of treatment have been described, no systematic-in depth- natural history studies exist using a route more likely to be encountered during an outbreak. By using different virus doses via the conjunctival route, we provide details of a novel mucosal challenge model that can be used to interrogate survivor versus lethal EVD signatures, evaluate medical countermeasures, and investigate viral latency.

Materials and methods

Challenge virus. The EBOV Makona variant seed stock originated from serum from a fatal case during the 2014 outbreak in Guékédou, Guinea (Ebola virus/H.sapiens-wt/GIN/2014/Makona-C07, accession number KJ660347.2) and was passaged twice in authenticated Vero E6 cells obtained from ATCC (ATCC, CRL-1586)[37,60]. Challenge inoculum was prepared by diluting the virus seed stock to the desired dose in sterile Hank's buffered saline solution (HBSS) with a final concentration of 2% fetal bovine serum (FBS) in 100 µL final volume.

Animal challenge. Animal studies were completed under Biosafety Level 4 containment at the Galveston National Laboratory (GNL) and were approved by the University of Texas Medical Branch (UTMB) IACUC, in accordance with state and federal statutes and regulations relating to experiments involving animals, and the UTMB Institutional Biosafety Committee. Eighteen healthy adult cynomolgus macaques (*Macaca fascicularis*) of Chinese origin (weight range, 4.3–7.0 kg; age range, 4–8 years; PreLabs) were used for these studies. Three sex-balanced challenge cohorts were established with 6 animals per cohort. For continuous core body temperature measurements. NHPs were surgically implanted with DST micro-T implantable temperature loggers (Star-Oddi, Gardabaer, Iceland) prior to placement on study. The temperature loggers were programmed to take measurements every 10–15 min. NHPs were anesthetized with Ketamine (5–20 mg/kg IM) or Telazol (2–6 mg/kg) prior to all procedures. Each cohort was exposed to a target dose of 100, 500, or 10,000 PFU of EBOV Makona. Briefly, 50 µL of challenge inoculum was delivered dropwise to the medial canthus of each eye for a total of 100 µL per animal. The eyelid was pulled out slightly to create a pocket for the inoculum and ensure secure administration of the challenge material. All animal challenges were performed with at least two trained personnel in the room for safety and to verify each animal got the full intended dose. For each challenge cohort, animals underwent physical examinations and blood specimens were collected at the time of challenge (day 0) and on days 1, 2, 3, 4, 5, 6, 7, 8, 10, 14, 21, and 28 post infection. Animals were monitored daily and scored for disease progression with an internal filovirus scoring protocol approved by the UTMB Institutional Animal Care and Use Committee (IACUC) and the USAMRDC Animal Care and Use Review Office (ACURO). The scoring changes measured from baseline included posture/activity level, attitude/behavior, food and water intake, weight, respiration, and disease manifestations such as visible rash, hemorrhage, ecchymosis, or flushed skin. A score of ≥ 9 indicated that an animal met criteria for euthanasia. This study was not blinded. Any surviving animals were euthanized on day 28. Research was conducted in compliance with the Animal Welfare Act. Experiments involving animals adhered to principles stated in the Guide for the Care and Use of Laboratory Animals from the National Research Council. UTMB is fully accredited by the American Association for Accreditation of Laboratory Animal Care (AAALAC). Animals were euthanized when moribund or at the end of the study following the American Veterinary Medical Association (AVMA) accepted methods of euthanasia.

Hematologic and serum biochemical analysis. Total white blood cell counts, white blood cell differentials, red blood cell counts, platelet counts, hematocrit values, total hemoglobin concentrations, mean cell volumes, mean corpuscular volumes, and mean corpuscular hemoglobin concentrations were analyzed in blood specimens collected in tubes containing ethylenediaminetetraacetic acid, using a laser based hematologic analyzer (Beckman Coulter). Serum samples were tested for concentrations of albumin, amylase, alanine aminotransferase, aspartate aminotransferase, alkaline phosphatase, γ glutamyl transferase, glucose, cholesterol, total protein, total bilirubin, blood urea nitrogen, creatinine, and C-reactive protein by using a Piccolo point-of-care analyzer and Biochemistry Panel Plus analyzer discs (Abaxis). Citrated plasma samples were analyzed for coagulation parameters PT, APTT, thrombin time, and fibrinogen on the STart4 instrument using the PTT Automate, STA Neoplastine CI Plus, STA Thrombin, and Fibri-Prest Automate kits, respectively (Diagnostica Stago).

Detection of viremia and viral RNA. RNA was isolated from whole blood utilizing the Viral RNA mini-kit (Qiagen) using 100 µl of blood added to 600 µl of the viral lysis buffer. Primers and probe targeting the VP30 gene of EBOV were used for real-time quantitative PCR (RT-qPCR) with the following probes: EBOV, 6-carboxyfluorescein (FAM)-5′ CCG TCA ATC AAG GAG CGC CTC 3′-6 carboxytetramethylrhodamine (TAMRA) (Life Technologies).Viral RNA was detected using the CFX96 detection system (Bio-Rad Laboratories, Hercules, CA) in one-step probe RT-qPCR kits (Qiagen) with the following cycle conditions: 50 °C for 10 min, 95 °C for 10 s, and 40 cycles of 95 °C for 10 s and 57 °C for 30 s. Threshold cycle (CT) values representing viral genomes were analyzed with CFX Manager software, and the data are shown as genome equivalents (GEq) per milliliter. To create the GEq standard, RNA from viral stocks was extracted, and the number of strain-specific genomes was calculated using Avogadro's number and the molecular weight of each viral genome.

Virus titration was performed for by plaque assay with Vero E6 cells from all plasma samples as previously described[37,60]. Briefly, increasing tenfold dilutions of the samples were adsorbed to Vero E6 monolayers in duplicate wells (200 μL); the limit of detection was 25 PFU/mL.

Anti-EBOV GP IgG ELISA. Sera collected at the indicated time points were tested for anti-EBOV immunoglobulin G (IgG) antibodies by standard ELISA. For GP-specific IgG titers, MaxiSorp clear flat-bottom 96-well plates (44204 ThermoFisher, Rochester, NY) were coated overnight with 15 ng/well (0.15 mL) of recombinant EBOV Makona GPΔTM (ΔTM: transmembrane region absent; Integrated Biotherapeutics, Gaithersburg, MD) in a sodium carbonate/bicarbonate solution (pH 9.6). Antigen-adsorbed wells were subsequently blocked with 4% bovine serum antigen (BSA) in 1× PBS for at least two hours. Sera were initially diluted 1:100 and then two-fold through 1:12,800 in ELISA diluent (1% BSA in 1× PBS, and 0.2% Tween-20). For total IgG titers, plates were coated with irradiated EBOV-Makona antigen or normal Vero E6 antigen kindly provided by Dr. Thomas W. Ksiazek (UTMB). Sera were initially diluted 1:100 and then four-fold through 1:6400 in 3% BSA in 1× PBS. After a one-hour incubation, plates were washed six times with wash buffer (1× PBS with 0.2% Tween-20) and incubated for an hour with a 1:2500 dilution of horseradish peroxidase (HRP)-conjugated anti-rhesus IgM or IgG antibody (Fitzgerald Industries International, Acton, MA). RT SigmaFast O-phenylenediamine (OPD) substrate (P9187, Sigma, St. Louis, MO) was added to the wells after six additional washes to develop the colorimetric reaction. The reaction was stopped with 3 M sulfuric acid 5–10 min after OPD addition and absorbance values were measured at a wavelength of 492 nm on a spectrophotometer (Molecular Devices Emax system, Sunnyvale, CA). Absorbance values were normalized by subtracting normal/uncoated wells from antigen-coated wells at the corresponding serum dilution. For total IgG titers, a sum OD value > 0.6 was required to denote a positive sample. End-point titers were defined as the reciprocal of the last adjusted serum dilution with a value ≥ 0.20.

Histopathologic, immunohistochemical (IHC), and in situ hybridization (ISH) analyses. Necropsy was performed on all subjects. Tissue samples from major organs were collected for histopathological and IHC examination, immersion fixed in 10% neutral buffered formalin, and processed for histopathologic analysis as previously described[37,60]. For IHC analysis, specific anti-EBOV immunoreactivity was detected using an anti-EBOV VP40 protein rabbit primary antibody (Integrated BioTherapeutics) at a 1:4000 dilution. Tissue sections were processed for IHC analysis, using the Dako Autostainer (Dako). Secondary antibody used was biotinylated goat anti-rabbit IgG (Vector Laboratories) at 1:200 followed by Vector horseradish peroxidase streptavidin, R.T.U (Vector Laboratories) for 30 min. Slides were developed with Dako DAB chromagen (Dako) for 5 min and counterstained with hematoxylin for 45 s. Methods for visualization with red chromogen were identical, except Vector Streptavidin Alkaline Phosphatase (Vector Laboratories) was used at a 1:200 dilution for 20 min, and slides were developed with Bio-Red (Biopath Laboratories) for 7 min and counterstained with hematoxylin for 45 s. EBOV RNA ISH in formalin-fixed paraffin embedded (FFPE) tissues was performed on representative tissue sections of brain using the RNAscope 2.5 high definition (HD) RED kit (Advanced Cell Diagnostics, Newark, CA) according to the manufacturer's instructions. 20 ZZ probe pairs targeting the genomic EBOV nucleoprotein (NP) gene were designed and synthesized by Advanced cell Diagnostics (catalog 448581). After sectioning, deparaffinization with xylene and graded ethanol washes and peroxidase blocking, the sections were heated in RNAscope Target Retrieval Reagent Buffer (Advanced Cell Diagnostics catalogue 322000) for 45 min and then air-dried overnight. The sections were then digested with Protease IV (catalogue 322336) at 40 °C in the HybEZ oven (HybEZ, Advanced Cell Diagnostics catalogue 321711) for 30 min. Sections were exposed to ISH target probe and incubated at 40 °C in the HybEZ oven for 2 h. After rinsing, the signal was amplified using the manufacturer provided pre-amplifier and amplifier conjugated to alkaline phosphatase and incubated with a red substrate-chromogen solution for 10 min, counterstained with hematoxylin, air-dried, and coverslipped.

EBOV neutralization assay. Neutralization assays were performed by measuring plaque reduction in a constant virus:serum dilution format as previously described[61]. Briefly, a standard amount of EBOV strain Makona (~ 100 PFU) was incubated with serial two-fold dilutions of the serum sample for 60 min. The mixture was used to inoculate Vero E6 cells (ATCC, CRL-1586) for 60 min. Cells were overlaid with an agar medium, incubated for 7 days, and plaques were counted 48 h after neutral red staining. Endpoint titers were determined by the dilution of serum which neutralized 50% of the plaques ($PRNT_{50}$).

Bead-based multiplex immunoassays. The concentrations of circulating cytokines, chemokines, and other analytes were assayed using bead-based multiplex technology. Irradiated plasma samples were incubated with magnetic beads from Milliplex NHP cytokine premixed 23-plex panel (EMD Millipore, Billerica, MA) kits according to the recommendations provided. Analytes measured included IL-1β, IL-1 receptor antagonist (IL-1RA), IL-2, IL-4, IL-5, IL-6, IL-8, IL-10, IL-12/23 (p40), IL-13, IL-15, IL-17, IL-18, gamma interferon (IFN-γ), granulocyte colony-stimulating factor (G-CSF), granulocyte–macrophage colony-stimulating factor (GM-CSF), monocyte chemoattractant protein 1 (MCP-1), macrophage inflammatory protein 1α (MIP-1α), MIP-1β, tumor necrosis factor alpha (TNF-α), transforming growth factor alpha (TGF-α), soluble CD40 ligand (sCD40L), and vascular endothelial growth factor (VEGF). The concentrations in each plasma sample were measured using a Bioplex-200 array system (Bio-Rad, Hercules, CA).

Ethics statement. The experiments reported in this study were performed and are reported in accordance with the recommendations in the ARRIVE guidelines.

Data availability

The datasets generated and/or analyzed during the current study are available from the corresponding author (TWG) upon reasonable request.

References

1. Feldmann, H., Sanchez, A. & Geisbert, T. W. *Field's Virology* Vol. 6 (Lippincott Williams & Wilkins, 2013).
2. Coltart, C. E. *et al.* The Ebola outbreak, 2013–2016: Old lessons for new epidemics. *Philos. Trans. R. Soc. Lond. B Biol. Sci.* **372**(1721), 20160297 (2017).
3. McMullan, L. K. *et al.* Characterisation of infectious Ebola virus from the ongoing outbreak to guide response activities in the Democratic Republic of the Congo: A phylogenetic and in vitro analysis. *Lancet Infect. Dis.* **19**(9), 1023–1032 (2019).
4. Vossler, H. *et al.* Analysis of individual-level data from 2018–2020 Ebola outbreak in Democratic Republic of the Congo. *Sci. Rep.* **12**(1), 5534 (2022).
5. MaríSaéz, A. *et al.* Investigating the zoonotic origin of the West African Ebola epidemic. *EMBO Mol. Med.* **7**(1), 17–23 (2015).
6. Adjemian, J. *et al.* Outbreak of Marburg hemorrhagic fever among miners in Kamwenge and Ibanda Districts, Uganda, 2007. *J. Infect. Dis.* **204**(Suppl 3), S796–S799 (2011).
7. Bausch, D. G. *et al.* Marburg hemorrhagic fever associated with multiple genetic lineages of virus. *N. Engl. J. Med.* **355**(9), 909–919 (2006).
8. Amman, B. R. *et al.* Seasonal pulses of Marburg virus circulation in juvenile *Rousettus aegyptiacus* bats coincide with periods of increased risk of human infection. *PLoS Pathog.* **8**(10), e1002877 (2012).
9. Olival, K. J. & Hayman, D. T. Filoviruses in bats: current knowledge and future directions. *Viruses* **6**(4), 1759–1788 (2014).
10. Caron, A. *et al.* Ebola virus maintenance: If not (only) bats, what else?. *Viruses* **10**(10), 549 (2018).
11. Mbala-Kingebeni, P. *et al.* Ebola virus transmission initiated by relapse of systemic Ebola virus disease. *N. Engl. J. Med.* **384**(13), 1240–1247 (2021).
12. Keita, A. K. *et al.* Resurgence of Ebola virus in 2021 in Guinea suggests a new paradigm for outbreaks. *Nature* **597**(7877), 539–543 (2021).
13. WHO. Ebola haemorrhagic fever in Zaire, 1976. *Bull World Health Organ.* **56**(2), 271–293 (1978).
14. Stone, R. Russian scientist dies after Ebola lab accident. *Science* **304**(5675), 1225–1225 (2004).
15. Gunther, S. *et al.* Management of accidental exposure to Ebola virus in the biosafety level 4 laboratory, Hamburg, Germany. *J Infect Dis* **204**(Suppl 3), S785–S790 (2011).
16. Jacobs, M. *et al.* Post-exposure prophylaxis against Ebola virus disease with experimental antiviral agents: A case-series of health-care workers. *Lancet. Infect. Dis* **15**(11), 1300–1304 (2015).
17. Rubinson, L. From clinician to suspect case: My experience after a needle stick in an Ebola treatment unit in Sierra Leone. *Am. J. Trop. Med. Hyg.* **92**(2), 225–226 (2015).
18. Vetter, P. *et al.* Ebola virus shedding and transmission: Review of current evidence. *J. Infect. Dis.* **214**(suppl_3), S177–S184 (2016).
19. Fischer, W. A. II. & Wohl, D. A. Confronting Ebola as a sexually transmitted infection. *Clin. Infect. Dis.* **62**(10), 1272–1276 (2016).
20. Tomori, O. & Kolawole, M. O. Ebola virus disease: Current vaccine solutions. *Curr. Opin. Immunol.* **71**, 27–33 (2021).
21. Geisbert, T. W., Strong, J. E. & Feldmann, H. Considerations in the use of nonhuman primate models of Ebola virus and Marburg virus infection. *J. Infect. Dis.* **212**(Suppl 2), S91–S97 (2015).
22. Sullivan, N. J. *et al.* Accelerated vaccination for Ebola virus haemorrhagic fever in non-human primates. *Nature* **424**(6949), 681–684 (2003).
23. Alfson, K. *et al.* Intramuscular exposure of *Macaca fascicularis* to low doses of low passage- or cell culture-adapted Sudan virus or Ebola virus. *Viruses* **10**(11), 642 (2018).
24. Alfson, K. J. *et al.* Particle to plaque-forming unit ratio of Ebola virus influences disease course and survival in cynomolgus macaques. *J. Virol.* **89**(13), 6773–6781 (2015).
25. Woolsey, C. *et al.* Postexposure efficacy of recombinant vesicular stomatitis virus vectors against high and low doses of Marburg virus variant Angola in nonhuman primates. *J. Infect. Dis.* **218**(suppl_5), S582–S587 (2018).
26. Johnston, S. C. *et al.* Delayed disease in cynomolgus macaques exposed to Ebola virus by an intranasal route. *Front. Immunol.* **12**, 709772 (2021).
27. Brasel, T. *et al.* Mucosal challenge ferret models of Ebola virus disease. *Pathogens* **10**(3), 292 (2021).
28. Johnson, E. *et al.* Lethal experimental infections of rhesus monkeys by aerosolized Ebola virus. *Int. J. Exp. Pathol.* **76**(4), 227–236 (1995).
29. Geisbert, T. W. *et al.* Vesicular stomatitis virus-based vaccines protect nonhuman primates against aerosol challenge with Ebola and Marburg viruses. *Vaccine* **26**(52), 6894–6900 (2008).
30. Alves, D. A. *et al.* Aerosol exposure to the Angola strain of Marburg virus causes lethal viral hemorrhagic fever in cynomolgus macaques. *Vet. Pathol.* **47**(5), 831–851 (2010).
31. Reed, D. S. *et al.* Aerosol exposure to Zaire ebolavirus in three nonhuman primate species: Differences in disease course and clinical pathology. *Microbes Infect.* **13**(11), 930–936 (2011).
32. Alfson, K. J. *et al.* Development of a lethal intranasal exposure model of Ebola virus in the cynomolgus macaque. *Viruses* **9**(11), 319 (2017).
33. Jaax, N. K. *et al.* Lethal experimental infection of rhesus monkeys with Ebola-Zaire (Mayinga) virus by the oral and conjunctival route of exposure. *Arch. Pathol. Lab. Med.* **120**(2), 140–155 (1996).
34. Mire, C. E. *et al.* Oral and conjunctival exposure of nonhuman primates to low doses of Ebola Makona virus. *J. Infect. Dis.* **214**(suppl 3), S263–S267 (2016).
35. Marzi, A. *et al.* Delayed disease progression in cynomolgus macaques infected with Ebola virus Makona strain. *Emerg. Infect. Dis.* **21**(10), 1777–1783 (2015).
36. Marzi, A. *et al.* VSV-EBOV rapidly protects macaques against infection with the 2014/15 Ebola virus outbreak strain. *Science* **349**(6249), 739–742 (2015).
37. Mire, C. E. *et al.* Single-dose attenuated Vesiculovax vaccines protect primates against Ebola Makona virus. *Nature* **520**, 688–691 (2015).
38. Patel, A. *et al.* Protective efficacy and long-term immunogenicity in cynomolgus macaques by Ebola virus glycoprotein synthetic DNA vaccines. *J. Infect. Dis.* **219**(4), 544–555 (2018).
39. Marzi, A. *et al.* Single low-dose VSV-EBOV vaccination protects cynomolgus macaques from lethal Ebola challenge. *EBioMedicine* **49**, 223–231 (2019).
40. Versteeg, K. *et al.* Infection with the Makona variant results in a delayed and distinct host immune response compared to previous Ebola virus variants. *Sci. Rep.* **7**(1), 9730 (2017).
41. Kwok, Y. L., Gralton, J. & McLaws, M. L. Face touching: A frequent habit that has implications for hand hygiene. *Am. J. Infect. Control* **43**(2), 112–114 (2015).

42. Nicas, M. & Best, D. A study quantifying the hand-to-face contact rate and its potential application to predicting respiratory tract infection. *J. Occup. Environ. Hyg.* **5**(6), 347–352 (2008).
43. Suarez, S. D. & Gallup, G. G. Face touching in primates: A closer look. *Neuropsychologia* **24**(4), 597–600 (1986).
44. Fischer, R. *et al.* Ebola virus stability on surfaces and in fluids in simulated outbreak environments. *Emerg. Infect. Dis.* **21**(7), 1243–1246 (2015).
45. Piercy, T. J. *et al.* The survival of filoviruses in liquids, on solid substrates and in a dynamic aerosol. *J. Appl. Microbiol.* **109**(5), 1531–1539 (2010).
46. Bielory, L. Allergic and immunologic disorders of the eye. Part I: immunology of the eye. *J. Allergy Clin. Immunol.* **106**(5), 805–816 (2000).
47. Bolanos-Jimenez, R. *et al.* Ocular surface as barrier of innate immunity. *Open Ophthalmol. J.* **9**, 49–55 (2015).
48. Corthesy, B. Multi-faceted functions of secretory IgA at mucosal surfaces. *Front. Immunol.* **4**, 185 (2013).
49. Coyle, P. K. & Sibony, P. A. Tear immunoglobulins measured by ELISA. *Investig. Ophthalmol. Vis. Sci.* **27**(4), 622–625 (1986).
50. Saw, V. P. *et al.* Conjunctival interleukin-13 expression in mucous membrane pemphigoid and functional effects of interleukin-13 on conjunctival fibroblasts in vitro. *Am. J. Pathol.* **175**(6), 2406–2415 (2009).
51. De Paiva, C. S. *et al.* Homeostatic control of conjunctival mucosal goblet cells by NKT-derived IL-13. *Mucosal Immunol.* **4**(4), 397–408 (2011).
52. Rogers, K. J. *et al.* IL-4/IL-13 polarization of macrophages enhances Ebola virus glycoprotein-dependent infection. *PLoS Negl. Trop. Dis.* **13**(12), e0007819 (2019).
53. Woolsey, C. *et al.* Immune correlates of postexposure vaccine protection against Marburg virus. *Sci. Rep.* **10**(1), 3071 (2020).
54. Zeng, X. *et al.* Identification and pathological characterization of persistent asymptomatic Ebola virus infection in rhesus monkeys. *Nat. Microbiol.* **2**, 17113 (2017).
55. Mate, S. E. *et al.* Molecular evidence of sexual transmission of Ebola virus. *N. Engl. J. Med.* **373**(25), 2448–2454 (2015).
56. Billioux, B. J., Smith, B. & Nath, A. Neurological complications of Ebola virus infection. *Neurotherapeutics* **13**(3), 461–470 (2016).
57. Shantha, J. G., Yeh, S. & Nguyen, Q. D. Ebola virus disease and the eye. *Curr. Opin. Ophthalmol.* **27**(6), 538–544 (2016).
58. Liu, J. *et al.* Ebola virus persistence and disease recrudescence in the brains of antibody-treated nonhuman primate survivors. *Sci. Transl. Med.* **14**(631), eabi5229 (2022).
59. Mire, C. E. & Geisbert, T. W. Evaluation of medical countermeasures against ebolaviruses in nonhuman primate models. *Methods Mol. Biol.* **1628**, 293–307 (2017).
60. Thi, E. P. *et al.* Lipid nanoparticle siRNA treatment of Ebola-virus-Makona-infected nonhuman primates. *Nature* **521**(7552), 362–365 (2015).
61. Jones, S. M. *et al.* Live attenuated recombinant vaccine protects nonhuman primates against Ebola and Marburg viruses. *Nat. Med.* **11**(7), 786–790 (2005).

Author contributions

R.W.C. and T.W.G. conceived and designed the animal challenge experiments. R.W.C., D.J.D., J.B.G., and T.W.G. performed the animal procedures and conducted clinical observations. K.N.A. and V.B performed the clinical pathology. K.N.A. performed the PCR and cytokine/chemokine assays. J.B.G. performed the EBOV infectivity assays. C.W. performed the ELISAs and neutralization assays. N.S.D. performed the IHC and ISH assays and developed the ISH assay. K.A.F. performed gross pathologic, histologic, and immunohistochemical analysis of the data. All authors analyzed the data. R.W.C., A.N.P., K.F., and T.W.G. wrote the paper. C.W. edited the paper. All authors had access to the data and approved the final version of the manuscript.

Competing interests

The authors declare no competing interests.

Additional information

Supplementary Information The online version contains supplementary material available at https://doi.org/10.1038/s41598-023-31027-7.

Correspondence and requests for materials should be addressed to T.W.G.

Reprints and permissions information is available at www.nature.com/reprints.

Publisher's note Springer Nature remains neutral with regard to jurisdictional claims in published maps and institutional affiliations.